A Novel Technique for Penetrator Velocity Measurement and Damage Identification in Ballistic Penetration Experiments

HORACIO D. ESPINOSA,* HUNG-CHENG LU AND YUEPING XU
School of Aeronautics and Astronautics
Purdue University
West Lafayette, IN 47907-1282

(Received July 3, 1996)
(Revised June 13, 1997)

ABSTRACT: A novel experimental configuration that can simultaneously record projectile velocity histories and target back surface out-of-plane motion in penetration experiments has been developed. The technique was used to investigate failure mechanisms during ballistic impact of an S-2 glass fiber woven composite with 60% fiber volume fraction. Microscopy studies performed on recovered samples clearly show interply delamination, fiber breakage, ply inelasticity, and fiber kinking as the major failure modes in these composites. Recorded penetrator velocity histories indicate the failure process is rate dependent.

Three well defined regions with different failure zones are observed in the laminate. In a region at the rear of the target plate, Region A, extensive delamination between plies is seen leading to bulge formation. Damage is observed in front of the penetrator with substantial fiber shearing. In a middle region, Region B, tensile fiber failure and large fiber deflection, to accommodate the lateral expansion generated by the steel penetrator, are observed. At the projectile entrance, Region C, fiber microfracture followed by fiber tensile failure is believed to be the failure mode in this region. Noticeable delamination is also produced in plies close to the front specimen surface. Two major fiber failure modes are observed in the micrographs, fiber kinking and cracking. Well defined kink bands are seen in Regions B and C on plies with fibers oriented perpendicular to the penetration direction. The formation of kink bands appears to be the result of compressive failure due to lateral motion of the plies away from the advancing steel penetrator.

KEY WORDS: interferometry, failure mechanisms, glass fiber woven composites, ballistic penetration.

*Author to whom correspondence should be addressed.

1. INTRODUCTION

IMPACT DAMAGE IN fiber-reinforced composite structures has received significant attention in the last decade. Fiber composite materials play an important role in civil and military applications through the design and manufacturing of advanced materials capable of attaining high stiffness/density and strength/density ratios. Presently, the utilization of glass fiber reinforced plastics (GRP) in the design of weight efficient armor systems and combat vehicles seems very promising. In these cases, analysis of structural integrity and dynamic response requires the understanding of failure mechanisms when fiber composites are subjected to high loading rates. Of particular interest is the problem of damage initiation and evolution in ballistic penetration.

In recent years, many studies have been undertaken to gain insight into the failure mechanisms induced by impact damage in fiber-reinforced composite materials (Abrate 1991, 1994, and Cantwell and Norton, 1991). In these studies, failure modes including delamination, interlaminar matrix cracking, fiber/matrix debonding, fiber breakage and fiber pull-out were observed. These findings prompted the need for investigations dealing with damage resistance and damage tolerance of composites.

In relation to the penetration resistance of fiber composites, two different velocity regimes were identified. Low velocity impact, e.g., when tools are dropped on the structure during maintenance operation or when debris is flying in a runway during take-off or landing, results in matrix fracture and interply delamination. In high impact velocity impact, e.g., penetrators striking a composite structure, other failure modes involving extensive fiber fracture and microbuckling are observed. In the latter case, the magnitude and extent of damage is a function of the penetrator shape and mass, striking velocity, plate thickness, and composite constituents' properties.

The overall energy absorbing ability of composite materials depends on properties of the composite components which include fibers, matrix, fiber-matrix interface and interface between plies. For instance, composites with higher fiber strength provide better impact resistance (Broutman and Rotem, 1975). Beaumont (1979) examined the energy involved in processes such as debonding and fiber pull-out to evaluate the low impact resistance of composites. He concluded that post-debond fiber sliding appears to be the primary energy absorbing mechanism in glass fiber-reinforced composites, whereas fiber pull-out is responsible for much of the toughness in a carbon fiber composite.

The role of matrix properties is not fully understood. High velocity impact tests conducted by Husman et al. (1975) showed that impact resistance has little dependence on matrix toughness. On the other hand, Williams and Rhodes (1982) found that the tensile performance of the matrix material has a significant effect on impact behavior. Hunston (1984) studied the link between matrix properties and fracture toughness. He showed that resin toughness is fully transferred to the toughness of the composite for brittle polymers, but for tougher polymers resin toughness is only partially transferred to the composite. Experimental results reported by Elber (1985) indicate matrix properties govern the damage threshold

and determine the extent of impact damage; while fiber properties control penetration resistance.

Strength of the interface between matrix and fiber also plays an important role in overall composite resistance to perforation and penetration. Dorey (1980) and Ying (1983) showed that transverse fracture energy of a composite depends significantly on fiber/matrix bond strength. Studies conducted by Peiffer (1979) indicated that impact resistance of glass-epoxy can be significantly improved by introducing a rubbery interface between the glass fibers and the rigid epoxy matrix. Modifications to the interface between plies for better penetration resistance were suggested by the analysis of Sun and Rechak (1988). Their stress analysis showed that introduction of an adhesive layer at the ply interface reduces interlaminar shear stresses during impact. Another technique that has been used successfully to delay and reduce delamination is stitching. Pelstring and Madan (1989) showed that stitching reduces the slope of the damage area as a function of impact energy. Moreover, as spacing between stitching decreases, the strain energy release rate G increases.

Lee and Sun (1933a and b) studied the static and dynamic penetration of fiber composites following a unique approach. Quasi-static penetration experiments performed on AS4/PEEK composites were used to investigate damage mechanisms and the load-deflection relation during penetration. They observed that damage initiates due to debonding followed by plug formation and pull-out of the plug. These findings under quasi-static conditions were successfully incorporated into a dynamic impact analysis to predict the ballistic limit of graphite/epoxy laminates without the need of performing impact tests. This approach does not seem to be applicable to glass fiber reinforced plastics (GRP) because failure in these materials is rate dependent.

It is well known that understanding the penetration resistance of materials requires measurement of penetrator force histories or alternatively its velocity history during the penetration event. Penetrator velocity measurements were performed with a streak camera, by adding a tail to the body of the projectile (Bless and Hartman, 1989; Bless et al., 1990). This technique is sometimes referred to as optical displacement technique. Since displacement histories are obtained, double differentiation is needed for the calculation of force histories. Recently, laser-Doppler anemometry (LDA) was applied to the measurement of projectile velocity histories (Wu et al., 1993). In contrast to the optical displacement method, LDA requires only one differentiation resulting in less noisy and more accurate force histories. Another attempt to measure penetrator force histories consisted of the use of reverse impact, in which a target plate is launched against a stationary projectile, and the utilization of an embedded manganin gauge within the projectile (Azzi et al., 1992). This method has the advantage that no differentiation of data is required for the determination of the force history.

In the present study a new technique for recording projectile velocity histories using a normal velocity interferometer (NVI) is presented. The study focuses on the comprehensive understanding of dynamic failure mechanisms in woven fiber-reinforced plastic laminates (GRP). The laminates are made of S-2 glass fibers embedded in a polyester resin matrix with approximately 60% fiber by vol-

ume. The penetration resistance of GRP was investigated through direct measurement of impactor tail velocity and the simultaneous measurement of target back surface velocity histories. Reverse penetration experiments were also performed to examine the penetrator velocity histories recorded in direct penetration experiments. Damage mechanisms in the penetration experiments were identified through detail microscopy studies performed on recovered composite samples.

2. PENETRATION EXPERIMENTS

In many ballistic impact tests, often only the incident and residual velocities are recorded. To understand how targets defeat projectiles, the complete velocity history of the projectile must be recorded. Moreover, multiple instrumentation systems are highly desirable because they provide enough measurements for the identification of failure through modeling and analysis. In this section we present a new experimental configuration that can record tail velocity histories of penetrators and target back surface out-of-plane motion in penetration experiments. The technique provides multiple real time diagnostics that can be used in model development. Laser interferometry is utilized to measure the surface motion of both projectile tail and target plate with nanosecond resolution.

2.1 Experimental Set-Up

Penetration experiments were conducted with a 3-in light gas gun with keyway at Purdue University. The experiments were designed to avoid complete destruction of the target plate so that microscopy studies could be performed in the samples. We have successfully measured impactor tail velocity and back surface target plate velocity histories by using the set-ups shown in Figures 1 and 2, direct and reverse penetration experiments, respectively.

In the case of direct penetration experiments (Figure 1) the projectile holder was designed such that a normal velocity interferometer could be obtained on a laser beam reflected from the back surface of the projectile. In addition to this measurement, a multi-point interferometer was utilized to continuously record the motion of the target back surface. It should be noted that the NVI system used in this configuration has variable sensitivity so its resolution can be adjusted to capture initiation and evolution of failure. The NVI records contain information on interply delamination, fiber breakage and kinking, and matrix inelasticity as these events start and progress in time.

A cylindrical target plate, 4 inches in diameter and 1 inch thick, was positioned in a target holder with alignment capabilities. The target was oriented so that impact at normal incidence was obtained. A steel penetrator, with a 30° conical tip, was mounted in a fiberglass tube by means of a PVC holder. This holder contained two mirrors and a plano-convex lens along the laser beam path. The focal distance of the plano-convex lens was selected to focus the beam at the penetrator back surface. Penetrator tail velocities were measured by means of the normal velocity interferometer (NVI), with signals in quadrature, shown in Figure 1. The interferometer beams were aligned while the penetrator was at the end of the gun barrel,

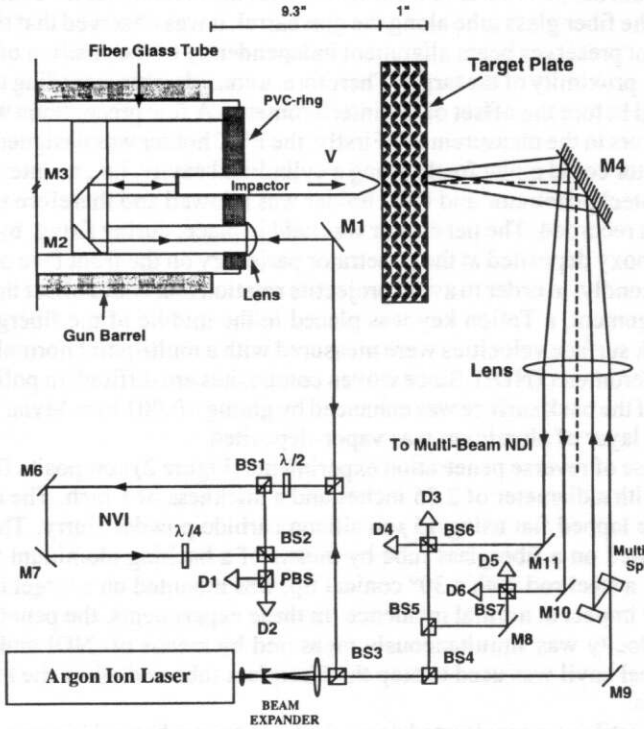

Figure 1. Experimental set-up for direct penetration experiments.

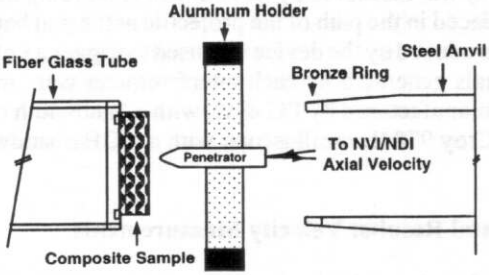

Figure 2. Experimental set-up for reverse penetration experiments.

i.e., on conditions similar to the conditions occurring at the time of impact. The alignment consisted in adjusting mirrors M1, M2, and M3 such that the laser beam, reflected from the penetrator tail, coincided with the incident laser beam. Through motion of the fiber glass tube along the gun barrel, it was observed that the present arrangement preserves beam alignment independently of the position of the penetrator in the proximity of the target. Therefore, a considerable recording time could be expected before the offset of the interferometer. A few precautions were taken to avoid errors in the measurement. Firstly, the PVC holder was designed such that the penetrator could move freely along a cylindrical cavity, i.e., no interaction between the steel penetrator and PVC holder was allowed and therefore true deceleration was recorded. The penetrator was held in place, during firing, by means of 5 minute epoxy deposited at the penetrator periphery on the front face of the PVC holder. Secondly, in order to avoid projectile rotation that could offset the interferometer alignment, a Teflon key was placed in the middle of the fiberglass tube. Target back surface velocities were measured with a multi-point normal displacement interferometer (NDI). Since woven composites are difficult to polish, the reflectivity of the back surface was enhanced by gluing a 0.001 inch Mylar sheet, and then a thin layer of aluminum was vapor-deposited.

In the case of reverse penetration experiments (Figure 2) composite flyer plates were cut with a diameter of 2.25 inches and a thickness of 1 inch. The composite plates were lapped flat using 15 μm silicon carbide powder slurry. These plates were mounted on a fiberglass tube by means of a backing aluminum plate. The penetrator, a steel rod with a 30° conical tip, was mounted on a target holder and aligned for impact at normal incidence. In these experiments, the penetrator back surface velocity was simultaneously measured by means of NDI and NVI systems. A steel anvil was used to stop the fiberglass tube and allow the recovery of the samples.

The projectile was accelerated down the keyway gun barrel by nitrogen gas filling a wrap-around breech. An aluminum piston with two rubber O-rings was mounted to the rear end of the fiber glass tube to seal the wrap-around breech. The projectile velocity was measured by electrinically recording the times of contact of four wire pins placed in the path of the projectile at the gun barrel exit. The first of the 1 volt steps produced by the device was used to trigger a LeCroy 9784L oscilloscope. The signals generated by each interferometer were monitored by silicon photodetectors manufactured by EG & G, with a bandwidth of 800 MHz, and recorded by a LeCroy 9784L oscilloscope with a 1 GHz bandwidth for 1 millisecond.

2.2 Experimental Results: Velocity Measurements

A summary of performed experiments is given in Table 1. The NVI signals in quadrature were analyzed following the procedure described in Barker (1980). The NDI signals were converted to particle velocities according to the following procedure. The interference fringes were filtered using a fast Fourier transform method and a cut-off frequency higher than the maximum fringe frequency. Furthermore, since the signal amplitude does not contain displacement information, it

Table 1. Summary of experiments.

Experiment Number	Impact Velocity [m/sec]	Specimen Dimensions [in]	Impactor Dimensions [in]	Type of Experiment
5-1122	200*	4″ dia. 1″ thick	0.56″ dia. 30° conical 2.5″ long	direct penetration
6-0308	200*	2.25″ dia. 1″ thick	0.56″ dia. 30° conical 2.5″ long	reverse penetration
6-0314	500*	2.25″ dia. 1″ thick	0.56″ dia. 30° conical 2.5″ long	reverse penetration
6-0531	181.6	4″ dia. 1″ thick	0.56″ dia. 30° conical 2.5″ long	direct penetration
6-1117	180.6	4″ dia. 1″ thick	0.56″ dia. 30° conical 2.5″long	direct penetration

*Velocity estimated from gas gun calibration curve based on breech pressure.

is customary to scale the signal to a constant amplitude prior to the displacement calculation. Hence, the filtered fringes were then scaled to obtain uniform fringe amplitude. Based on the displacement interferometer principles, one can assume that the interferometer signal consists of fringes in a sine-like function of voltage versus time, e.g., $y(t) = a(t) \sin [f(t)] + b(t)$, where $a(t)$ is the amplitude, $b(t)$ is the zero offset, and $f(t)$ is the phase function.

In general, $a(t)$ and $b(t)$ are not constant. They can be evaluated by finding the envelopes, $h(t)$ and $l(t)$, formed by peaks and valleys, respectively. These functions are given by $a(t) = 0.5\,[h(t) - l(t)]$ and $b(t) = 0.5\,[h(t) + l(t)]$ (Tong, 1991). The amplitude corrected signal, $y_0(t)$, is then determined by $y_0(t) = [\,y(t) - b(t)]/a(t)$. The signal phase function can be obtained from $f(t) = \arcsin [\,y_0(t)]$. Then the displacement can be computed from $d(t) = d_0 f(t)/2\pi$. The constant d_0 is a function of the interferometer; for an NDI, $d_0 = \lambda/2$. Velocities were obtained by differentiating the displacement histories numerically. All calculations were automatically performed with MATLAB. The functions MENU, GINPUT, INPUT, and STRCMP were used to input the data files. The functions FIR1 and FFTFILT were used to perform the fast Fourier transform filtering. The function INTERP1 was employed to fit the peaks and valleys with cubic splines. The function GRADIENT was utilized to perform the numerical differentiation.

The impactor velocity during the penetration event, in experiments 5-1122 and 6-1117, is given in Figure 3. A velocity reduction of approximately 32 m/sec in shot 5-1122 and about 20 m/sec in shot 6-1117 are observed after 100 μsec of the recorded impact. In shot 5-1122, a progressive decrease in velocity is observed in the first 30 μsec followed by an almost constant velocity and a sudden velocity increase of 7 m/sec at approximately 60 μsec. Further reduction in velocity is

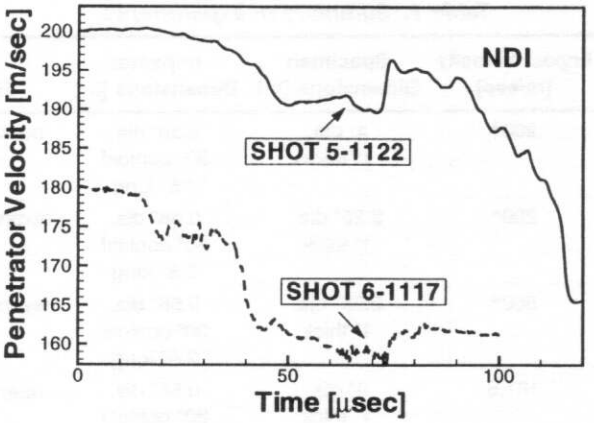

Figure 3. *Penetrator axial velocity recorded in experiments 5-1122 and 6-1117.*

measured in the next 40 μsec. In the case of shot 6-1117, the tail velocity shows a profile with features similar to the one recorded in shot 5-1122. These velocity histories present a structure that should be indicative of the contact forces that develop between penetrator and target, as well as the effect of damage in the penetration resistance of GRP target plates. It should be noted that a projectile traveling at 200 m/sec moves a distance of 20 mm in 100 μsec.

Back surface velocity histories at the specimen center, measured by means of a normal displacement interferometer (NDI), are shown in Figure 4 for shots 5-1122, 6-0531, and 6-1117. A velocity increase to a value of 22 m/sec, followed by a decrease and increase to a maximum velocity of about 50 m/sec, after 20 μsec, is

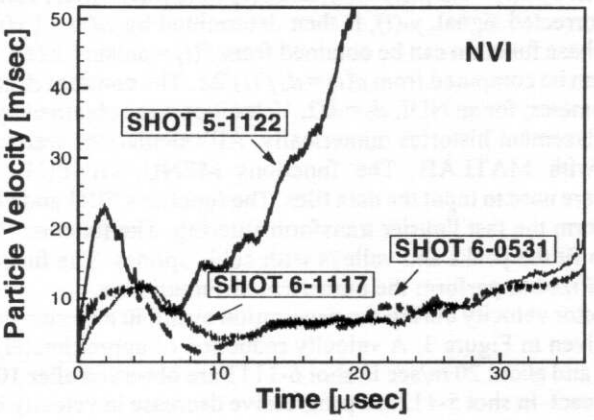

Figure 4. *Back surface normal velocity history at the center of the composite target, experiments 5-1122, 6-0531, and 6-1117.*

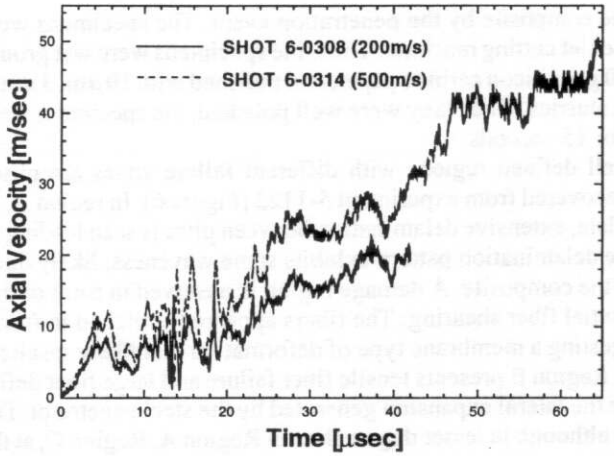

Figure 5. *Penetrator velocity histories from experiments 6-0308 and 6-0314.*

measured in shot 5-1122. The traces from shots 6-0531 and 6-1117 show features similar to the features present in the velocity history recorded in experiment 5-1122. However, significant differences in amplitude are observed. A maximum particle velocity of 18 m/sec is observed at about 37.5 μsec. These velocity histories present variations such as small humps with some apparent periodicity. Numerical simulation of the experiments, incorporating the observed failure modes, is required to interpret the various features observed in the velocity traces.

In order to confirm the velocities measured in the direct penetration experiment, we conducted two reverse penetration experiments at impact velocities of 200 and 500 m/sec (experiments 6-0308 and 6-0314, respectively). Another objective of these experiments was to examine rate effects in the penetration resistance of woven fiber composites. The interferometrically measured penetrator tail velocities are plotted in Figure 5. The steel penetrator velocity shows a progressive increase and a decrease to almost zero velocity upon arrival of an unloading wave generated at the penetrator free surface. The arrival time of approximately 14 μsec coincides with the round trip time of the wave through the penetrator nose back to the penetrator tail. This feature is observed in both experiments. A continuous increase in velocity is recorded with velocities of 20 m/sec and 32 m/sec after 42 μsec, respectively. A maximum velocity of 50 m/sec is recorded in experiment 6-0314 after 65 μsec. A comparison of the velocity histories in these two experiments clearly reveals that composite failure presents a moderate rate sensitivity. Moreover, the velocity recorded in experiment 6-0308 appears to confirm the velocity reduction interferometrically recorded in experiment 5-1122 (direct penetration experiment).

2.3 Microscopy Study: Failure Mechanisms

Recovered samples were examined under an optical microscope and a scanning electron microscope. The purpose of these studies was to observe the damage in-

duced in the composite by the penetration event. The specimens were sectioned using a water jet cutting machine. Then, the specimens were wet ground with 320, 400 and 600 grit silicon carbide paper, and polished with 10 μm, 3 μm, 0.1 μm alumina oxide slurries. Once they were well polished, the specimens were etched by 2.5 N HF for 15 seconds.

Three well defined regions with different failure zones are observed in the specimen recovered from experiment 5-1122 (Figure 6). In region A, at the rear of the target plate, extensive delamination between plies is seen leading to bulge formation. The delamination pattern exhibits some waveness, likely due to the morphology of the composite. A damage region is observed in front of the penetrator with substantial fiber shearing. The fibers appeared stretched in front of the projectile suggesting a membrane type of deformation that likely results in fiber tensile failure. Region B presents tensile fiber failure and large fiber deflection to accommodate the lateral expansion generated by the steel penetrator. Delamination is observed although in lesser degree than in Region A. Region C, at the projectile entrance, does not show extensive fiber deflection. Fiber microfracture followed by fiber tensile failure is believed to be the failure mode in this region. It should be pointed that this failure precedes and allows the penetration event. Noticeable delamination is also observed in plies close to the front specimen surface. In experiment 6-0531, in which the impact velocity was 181.6 m/sec, only partial penetration is observed (see Figure 7). The distribution of interply delamination is similar to that observed in experiment 5-1122. However, less fiber deflection and bulging are observed. The region in front of the penetrator clearly shows the onset of fiber tensile failure.

In addition to delamination, impact causes fiber failure, matrix cracking, and fiber-matrix debonding. Optical micrographs taken at the boundary between Re-

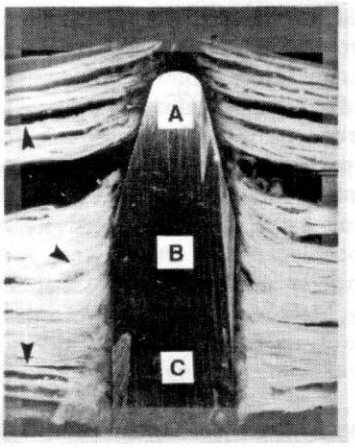

Figure 6. *Optical micrograph of recovered composite sample from direct penetration, experiment 5-1122. Three regions with different failure modes are observed. The half-inch diameter penetrator provides a scale for this micrograph.*

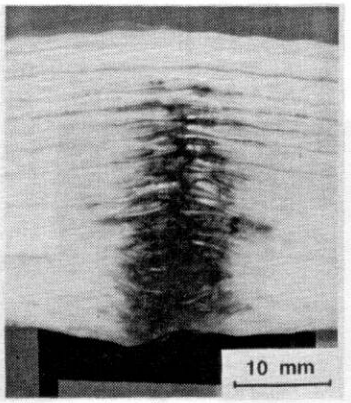

Figure 7. *Optical micrograph of recovered composite sample from direct penetration experiment 6-0531. The micrograph indicates that only partial penetration occurred.*

gions A and B, specimen from Shot 5-1122, show all these failure mechanisms (see Figures 8 and 9). Two major fiber failure modes are observed in the micrographs, fiber kinking and cracking. In Figure 8 a well defined kink band, on a ply with fibers oriented perpendicular to the penetration direction, is seen. Figures 10 and 11 show further evidence of well defined kink bands. In Figure 11, two kink bands are observed, one of them only partially developed. The development of kink bands appeared to be the result of compressive failure due to lateral motion of the plies away from the advancing steel penetrator. A schematic of the compression-shear stress state, believed to occur in this region, is shown in Figure 10. Many kink bands were observed in Regions B and C, but none were observed in Region A. The formation of kink bands was also observed in the recovered specimens from experiments 6-0531 and 6-1117.

Fiber bending and large fiber rotations are observed in Figure 9. A typical failure mode with fiber shearing and deflection is seen in the lower ply. Interply delamination seems to assist these types of instabilities when the plies are moved laterally by the projectile. It should be noted that in these figures the gap between 0°/90° plies is filled with glue. The glue was infiltrated in the recovered samples to avoid further damage in the composite and to facilitate the preparation of microscopy samples. Two SEM pictures showing details of fiber failure are shown in Figures 12 and 13. The extent of bending and the periodic formation of L and T-shaped cracks can be observed in Figure 13. The microcrack spacing is approximately 30–40 μm. These microcracks appear to initiate in the tensile region of the fiber propagating in a direction perpendicular to the fiber axis. A change in crack propagating direction, presumably due to stress wave interactions, is observed when the crack approaches the compressive region within each fiber. At this stage, crack extension parallel to the fiber axis is seen. This failure mechanism is consistent with the independent bending of each fiber, likely resulting from debonded fiber-matrix interfaces.

Shown in Figures 14 and 15 are SEM micrographs of a kink band observed in

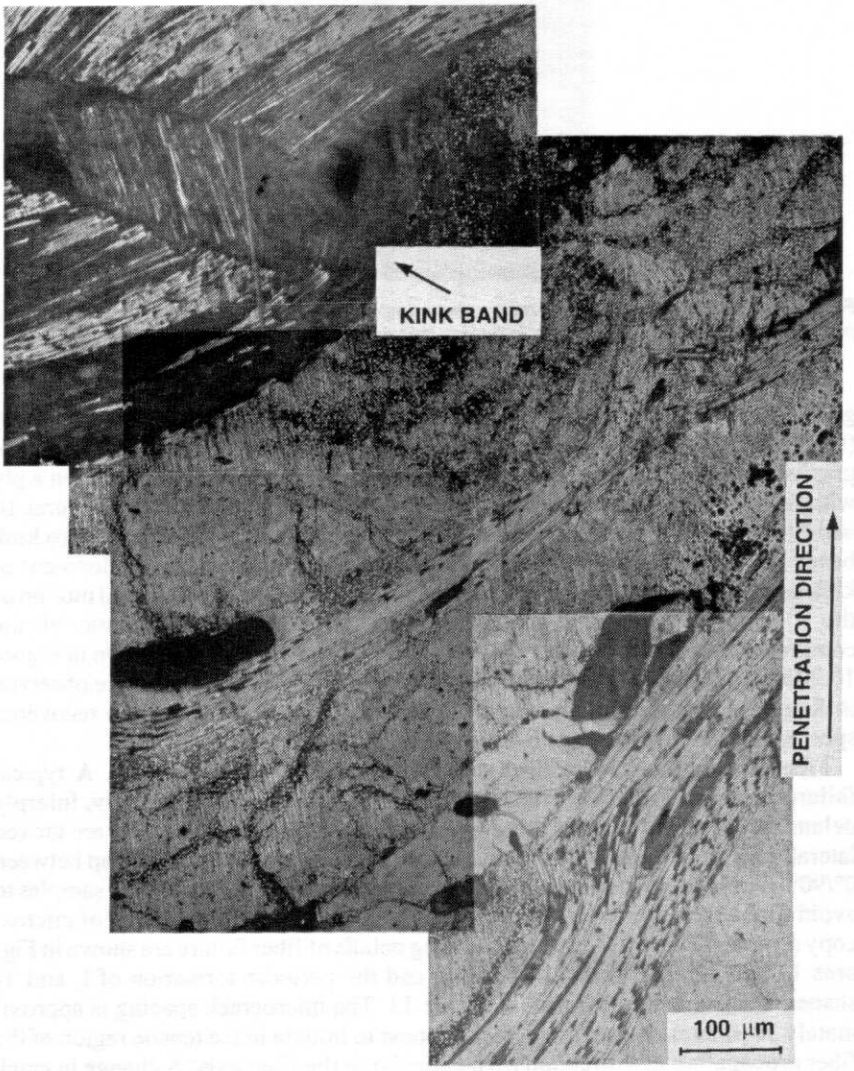

Figure 8. *Optical micrograph taken at the boundary between Regions A and B. Fiber kinking and matrix cracking are observed in 0° and 90° plies, respectively.*

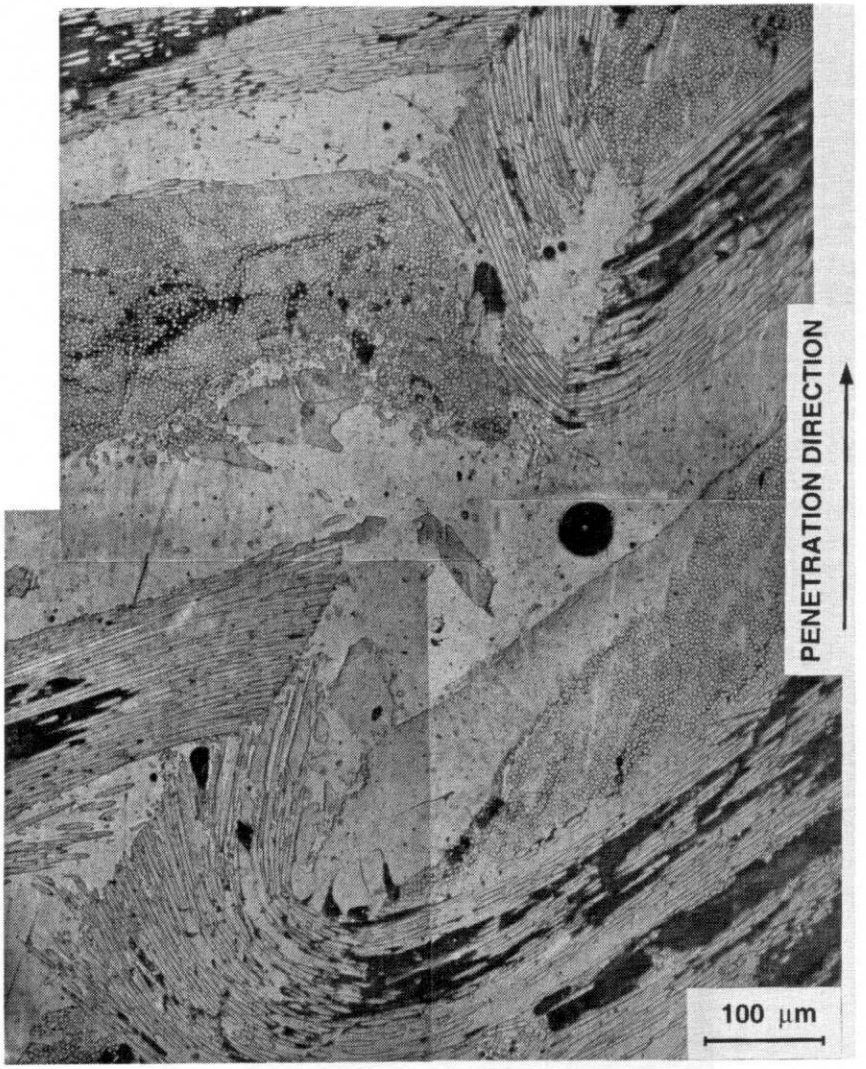

Figure 9. *Optical micrograph taken at the boundary between Regions A and B. Fiber shearing and bending with large displacements and rotations are observed.*

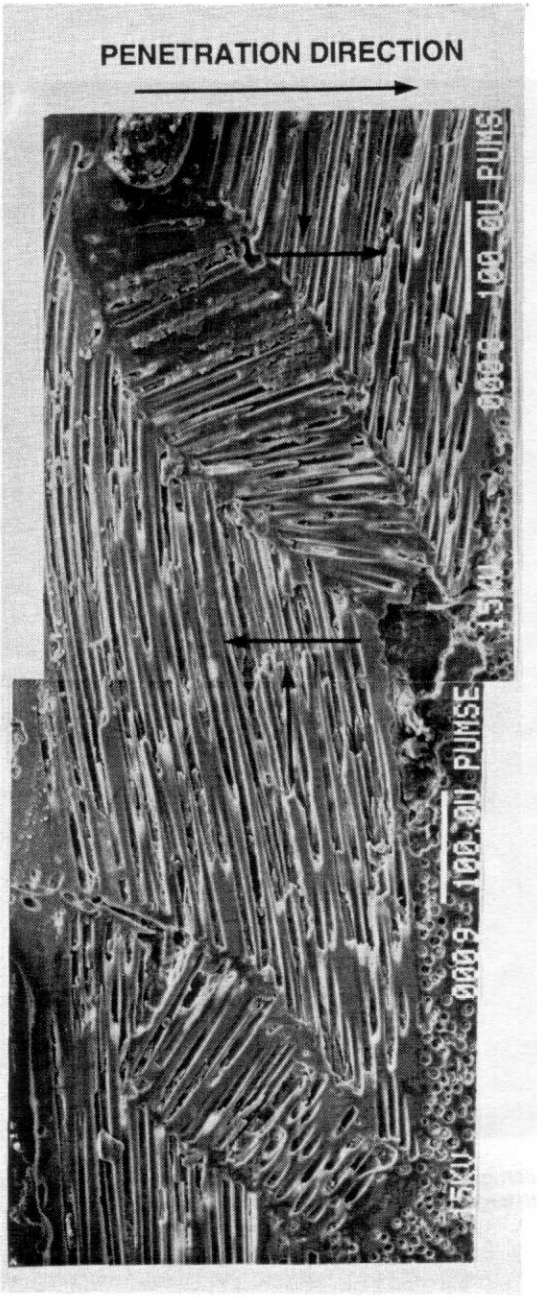

Figure 10. *SEM micrograph showing kink bands in specimen recovered from experiment 6-0531. Arrows are indicative of the compression-shear stress state generated by the advancing penetrator (not shown in the figure).*

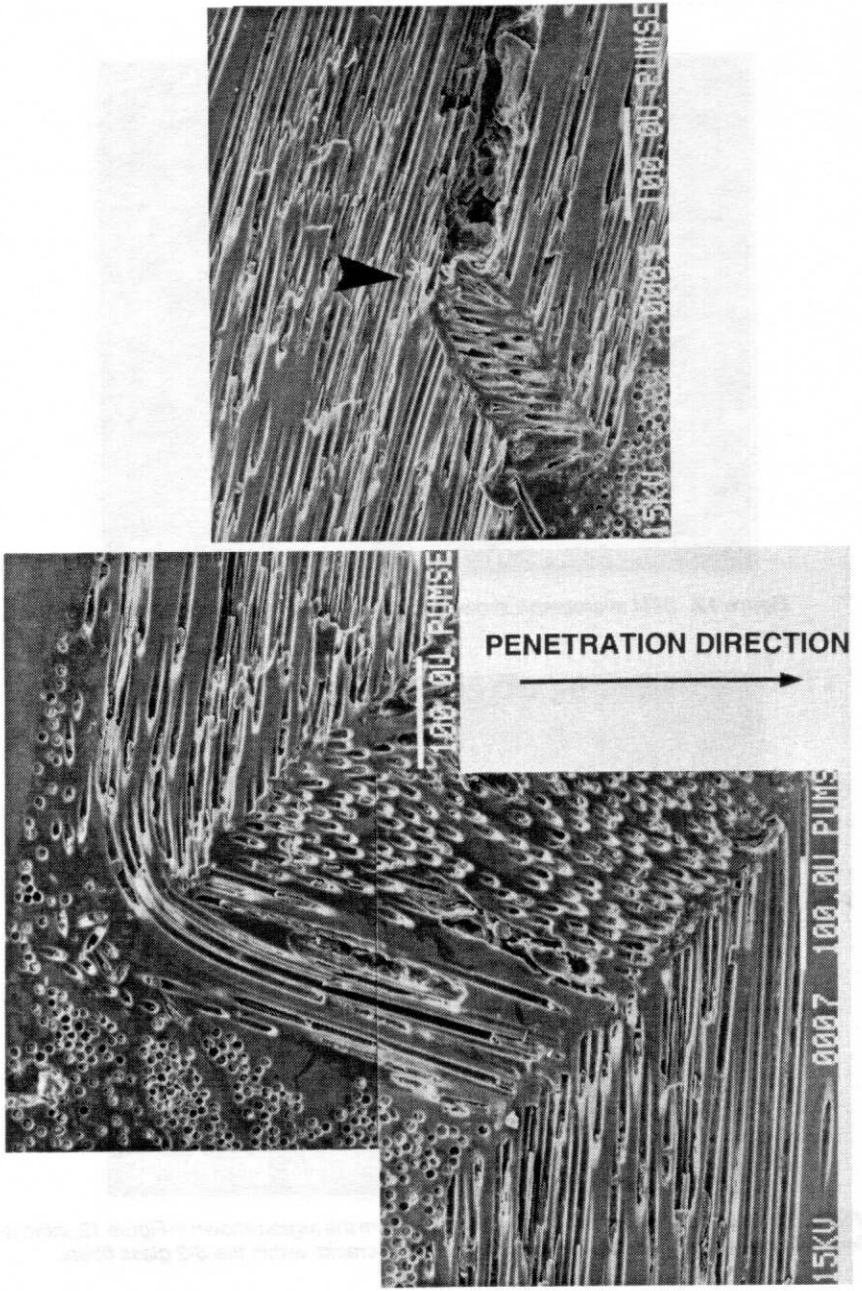

Figure 11. *SEM micrograph showing a partially developed kink band in specimen recovered from experiment 6-0531.*

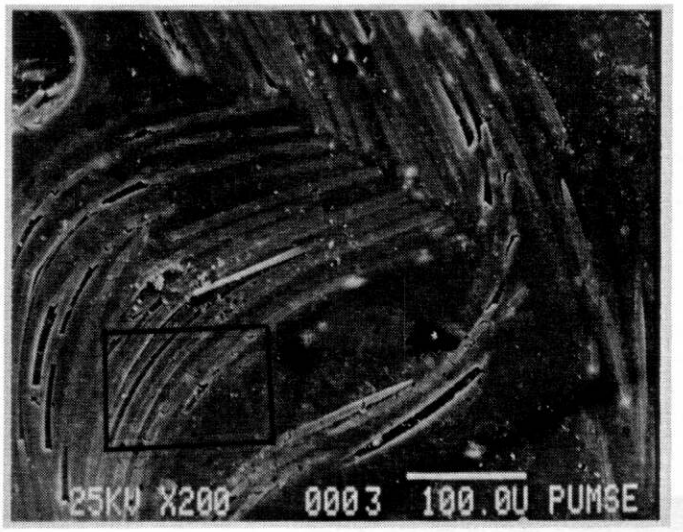

Figure 12. *SEM micrograph showing details of fiber bending and cracking.*

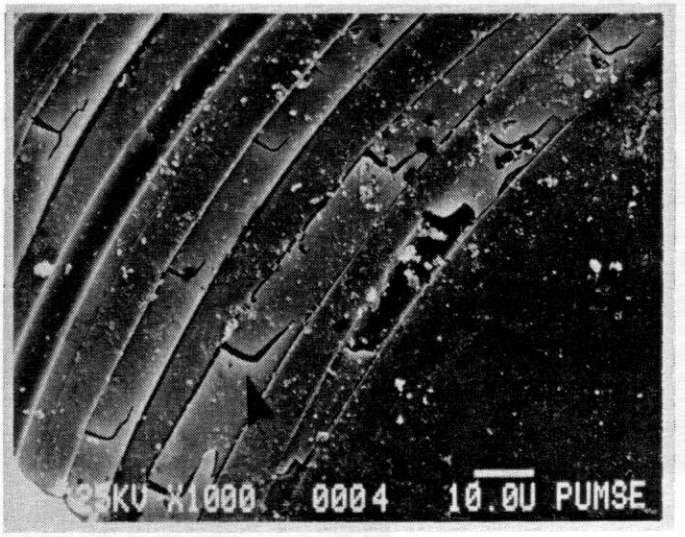

Figure 13. *High magnification SEM micrograph, from the region shown in Figure 12, indicating the formation of periodic L and T-shaped microcracks within the S-2 glass fibers.*

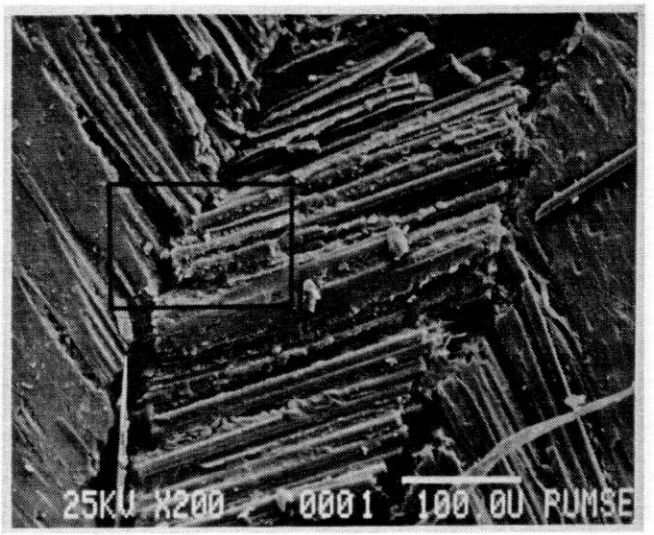

Figure 14. *SEM micrograph of a typical kink band showing a band width of approximately 250 μm, experiment 5-1122.*

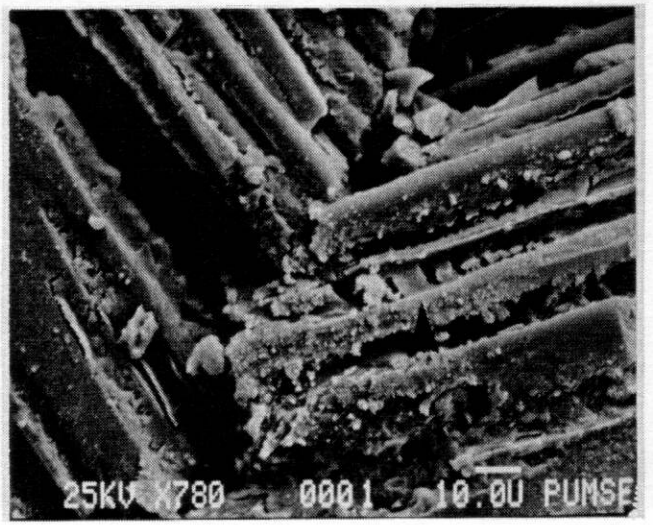

Figure 15. *High magnification SEM micrograph, from the region shown in Figure 14, displaying extensive fiber-matrix debonding and granular appearance of the polymer matrix.*

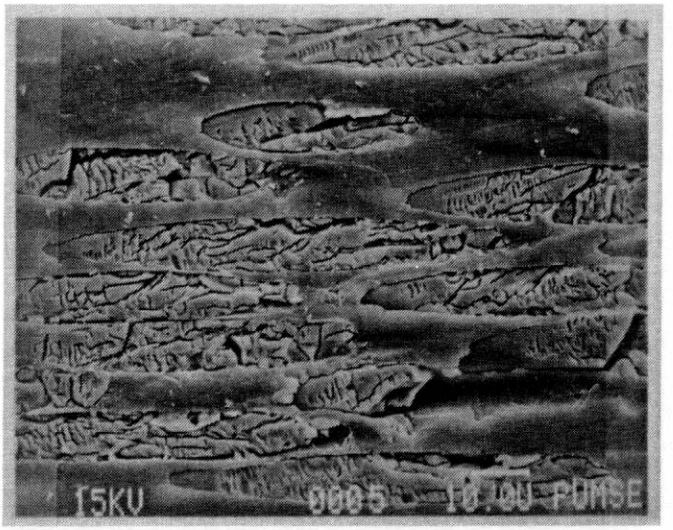

Figure 16. *SEM micrograph showing fiber pulverization at the penetrator entrance cavity.*

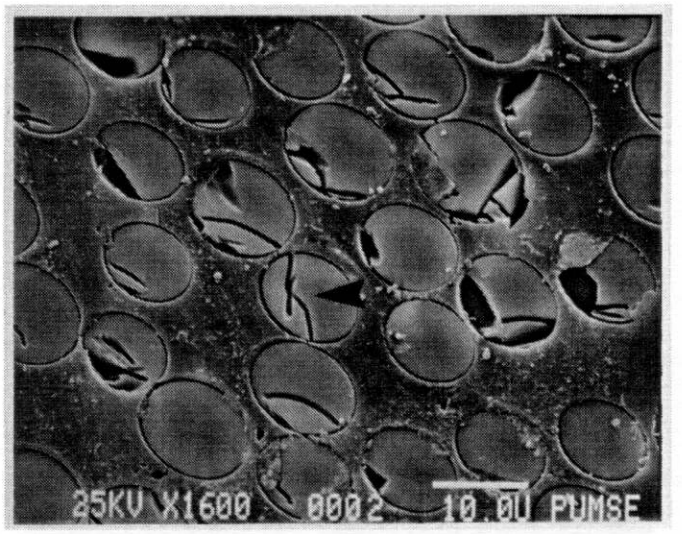

Figure 17. *SEM micrograph of a 90° ply taken in Region B, at 100 μm from the penetrator cavity. Severe fiber cracking and matrix-fiber debonding are observed.*

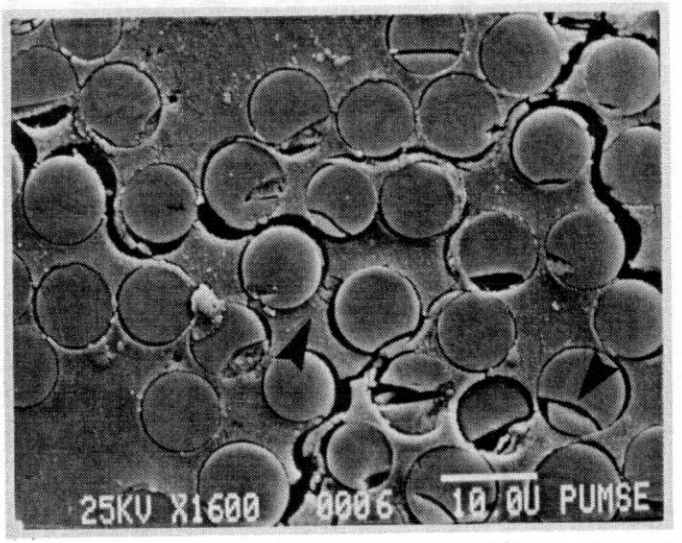

Figure 18. *SEM micrograph of a 90° ply taken in Region B, at 300 μm from the penetrator cavity. Matrix cracking with large openings is observed.*

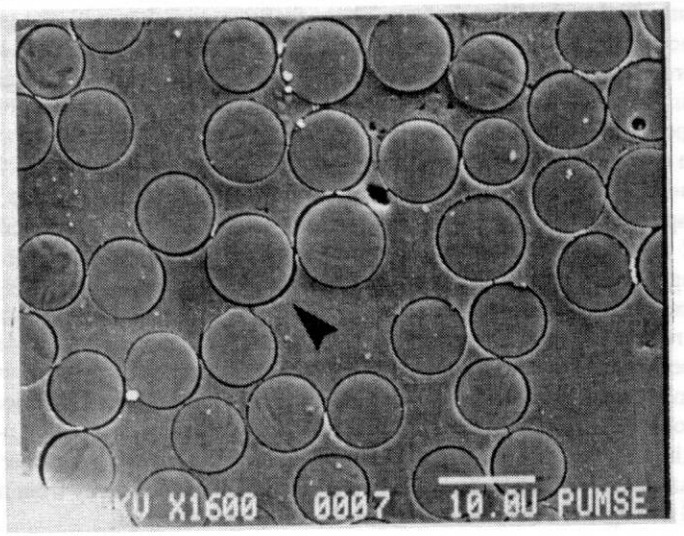

Figure 19. *SEM micrograph of a 90° ply taken in Region B, at 1000 μm from the penetrator cavity. No fiber breakage and small fraction of debonded fiber-matrix interphases is observed.*

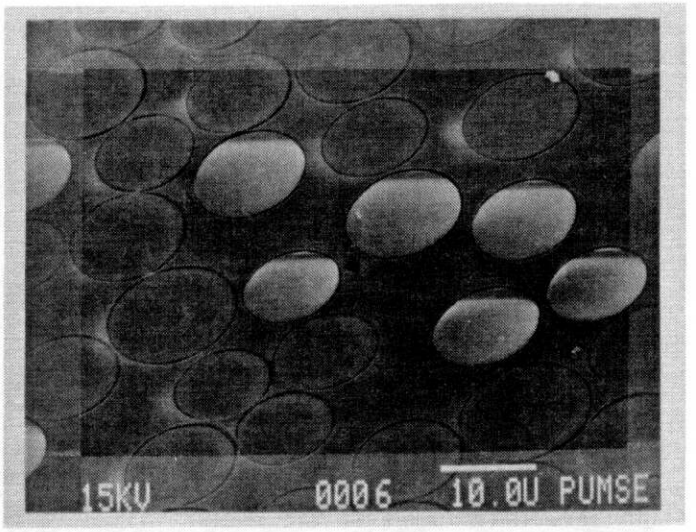

Figure 20. *SEM micrograph of untested sample.*

the specimen recovered from experiment 5-1122. A band width of approximately 250 μm is observed. The matrix has a granular appearance and presents large amounts of inelasticity. Extensive fiber-matrix debonding is seen with matrix material attached to the fiber surface. These features, together with the granular appearance of the polymer matrix, suggest heating and quenching of the polymer.

In order to examine the extent of damage in 90° plies, SEM micrographs were taken in Regions C and B. An SEM micrograph taken from a contact region close to the penetrator entrance cavity is shown in Figure 16. Fiber fracture with the formation of multiple fragments is observed. In Region B, micrographs 100 μm, 300 μm, and 1000 μm away from the penetrator cavity were taken (Figures 17, 18, and 19, respectively). Extensive fiber cracking and matrix-fiber debonding is observed in the region close to the penetrator cavity. Matrix cracking with large openings and moderate fiber cracking is observed 300 μm away from the penetrator. This feature is consistent with observations previously noted in Figures 8 and 9.

In a region 1000 μm away from the penetrator cavity, the appearance of the matrix and fiber-matrix interfaces is very similar to the appearance of untested material. An SEM micrograph of untested material is given in Figure 20 for reference purposes. These observations suggest ply damage is mainly contained in a region with a width approximately half the penetrator diameter on each side of the penetrator cavity. By contrast, interply delamination is extended several diameters away from the penetrator and in Region A involves the entire 4-inch target diameter.

3. CONCLUDING REMARKS

A novel experimental configuration that can record projectile tail velocity histories and target back surface out-of-plane motion in penetration experiments has

been developed. The experiment should provide information on failure mechanisms, their initiation and evolution, and their interaction in ballistic penetration studies. It is shown that a variety of failure modes is produced during penetration of thick laminates. The precise sequence of events and stresses leading to these failures can only be identified through 3-D numerical simulations of the penetration process. All measured velocity histories are instrumental in providing insight into the damage and failure processes.

The feasibility of measuring penetrator velocity histories in direct penetration experiments is shown. Moreover, the deceleration interferometrically recorded in these experiments is shown to be consistent and of the same order of magnitude as the penetrator acceleration recorded in reverse penetration experiments. It should be noticed that in the case of direct penetration the composite sample had a diameter of 4 inches, while in the case of the reverse penetration experiment the composite sample had a diameter of 2.25 inches. Based on the microscopy study previously reported, it is clear that the major difference between the 4 and 2.25-inch samples is in the extent of interply delamination. As noted earlier, damage and failure during the penetration event is confined to a dimension approximately half a penetrator diameter. Likely, this is the reason for reasonable agreement between direct and reverse projectile velocity measurements. Additional experiments are needed to confirm these findings.

The failure processes observed experimentally provide a clear picture of the main features that need to be addressed in the modeling of ballistic penetration of fiber composites. These are: 1) inelasticity within each individual ply accounting for fiber orientation, damage, rate, and temperature effects; 2) interply delamination in the presence of compressive normal tractions; 3) dynamic instabilities leading to fiber kinking (microbuckling); and 4) large deformation effects including large fiber displacements and rotations. All these failure modes should be incorporated in numerical analyses of the penetration event to interpret the interferometrically measured particle velocities. The analyses should provide information on the role of each failure mode and its synergy in the penetration resistance of fiber composites.

ACKNOWLEDGEMENTS

This research was supported by the National Science Foundation through Grant Nos. MSS-9309006 and MSS 9311289, and by the Army Office of Scientific Research under Grant DAAH 04-95-1-0168.

REFERENCES

Abrate, S. 1991. "Impact on Laminated Composite Materials," *Applied Mechanics Review*, 44(4):155–190.

Abrate, S. 1994. "Impact on Laminated Composites: Recent Advances," *Applied Mechanics Review*, 47(11):517–544.

Azzi, B., S. J. Bless and N. S. Brar. 1991. "Force Measurements on Projectiles Penetrating Fiber Reinforced Composite Targets," *Proc. 23rd Int. SAMPE Conf.*, pp. 616–623.

Barker, L. M. 1988. "VISAR88—A New Data Reduction Program for VISARs," *Sandia Report,* SAND88-2788.

Beaumont, P. W. R. 1979. "Fracture Mechanisms in Fibrous Composites," in *Fracture Mechanics, Current Status, Fracture Prospects,* R. A. Smith, ed., Pergamon Press, pp. 211–233.

Bless, S. J. and D. R. Hartman. 1989. "Ballistic Penetration of S-2 Glass Laminates," *Proc. 21st Int. SAMPE Conf.,* pp. 852–866.

Bless, S. J., M. Benyami and D. Hartman. 1990. "Penetration Through Glass-Reinforced Phenolic," *Proc. 22nd Int. SAMPE Conf.,* pp. 293–303.

Broutman, L. J. and A. Rotem. 1975. "Impact Strength and Toughness of Fiber Composite Materials," in *Foreign Object Impact Damage to Composites,* American Society for Testing and Materials, ASTM STP 568, pp. 114–133.

Cantwell, W. J. and J. Norton. 1991. "The Impact Resistance of Composite Materials—A Review," *Composites,* 22(5):347–362.

Dorey, G. 1980. "Relationship between Impact Resistant and Fracture Toughness in Advanced Composite Materials," in *Effect of Service Environment on Composite Materials,* AGARD CP 28.

Elber, W. 1985. "Failure Mechanics in Low Velocity Impact on Thin Composite Plates," *NASA Technical Paper 2152.*

Hunston, D. L. 1984. "Composite Interlaminar Fracture; Effect of Matrix Fracture Energy," *Composites Tech Review 6,* pp. 176–180.

Husman, G. E., J. M. Whitney and J. C. Halpin. 1975. "Residual Strength Characterization of Laminated Composites Subjected to Impact Loading," in *Foreign Object Impact Damage to Composites,* ASTM, STP 568, pp. 92–113.

Lee, S-W. R. and C. T. Sun. 1993a. "A Quasi-Static Penetration Model for Composite Laminates," *J. of Composite Materials,* 27:251–271.

Lee, S-W. R. and C. T. Sun. 1993b. "Dynamic Penetration of Graphite/Epoxy Laminates Impacted by a Blunt-Ended Projectile," *Composites Science and Technology,* 49:369–380.

Peiffer, D. G. 1979. "Impact Strength of Thick Interlayer Composites," *J. Appl. Polym. Sci.,* 24:1451–1455.

Pelstring, R. M. and R. C. Madan. 1989. "Stitching to Improve Damage Tolerance of Composites," *Proc. 34th Int. SAMPE Symp.,* pp. 1519–1528.

Sun, C. T. and S. Rechak. 1988. "Effect of Adhesive Layers on Impact Damage in Composite Laminates," American Society for Testing and Materials, ASTM STP 972, pp. 97–123.

Tong, W. 1991. "Pressure-Shear Impact Investigation of Strain-Rate History Effects in OFHC Copper," PhD Thesis, Brown University, Providence, RI.

Williams, J. G. and M. D. Rhodes. 1982. "Effect of Resin on Impact Damage Tolerance of Graphite/Epoxy Laminates" in *Composite Materials: Testing and Design (Sixth Conference),* American Society for Testing and Materials, I. M. Daniel, ed., ASTM STP 787, pp. 450–480.

Wu, E., H.-J. Sheen, Y.-C. Chen and L.-C. Chang. 1993. "Penetration Force Measurement of Thin Plates by Laser Doppler Anemometry," *Exp. Mech.,* pp. 93–99.

Ying, L. 1983. "Role of Fiber/Matrix Interphase in Carbon Fiber Epoxy Composite Impact Toughness," *SAMPE Quart.,* 14(3):26.